Journal of Hazardous Materials 170 (2009) 1023–1040

Contents lists available at ScienceDirect

Journal of Hazardous Materials

journal homepage: www.elsevier.com/locate/jhazmat

Mathematical modelling of slow pyrolysis of a particle of treated wood waste

J. Ratte[a,b], F. Marias[b,*], J. Vaxelaire[b], P. Bernada[b]

[a] THERMYA, 1 rue Nicolas Appert, VILLENAVE D'ORNON, France
[b] LaTEP-UPPA, LaTEP-ENSGTI, Rue Jules Ferry BP 7511, 64075 Pau, France

ARTICLE INFO

Article history:
Received 17 November 2008
Received in revised form 14 May 2009
Accepted 16 May 2009
Available online 22 May 2009

Keywords:
Treated wood
Waste
Pyrolysis
Porous media
Volume averaging method
Modelling

ABSTRACT

Low-temperature pyrolysis is a possible method for the disposal of wood waste treated with chromated copper arsenic (CCA). A mathematical model (heat and mass transfer) including chemical reactions of the thermal degradation of a particle of wood is presented. A spherical particle is heated by a convective nitrogen flow. The progress of the pyrolysis process is characterized by three main steps: (1) drying of the wet sample; (2) heating of the sample until ignition of pyrolysis reactions; (3) pyrolysis and subsequent production of char and volatiles. The mathematical model is based on the volume averaging concept and it uses Shafizadeh and Chin [F. Shafizadeh, P.S. Chin, Thermal deterioration of wood, wood technology: chemical aspects, ACS Symposium Series 43 (1977) 57–81] pyrolysis model to describe the reaction pathway.

It is solved by the line method, taking time as the preferred variable. Our model predicts intra-particle profiles for several variables (temperature, moisture content, concentration of wood). Simulations are presented with a spherical particle of 1 cm radius.

1. Introduction

When wood is used for outdoor applications (railways sleepers, electricity transmission poles), it is often treated with a preserving agent because it can be altered by external or internal mechanisms like insect, fungi, rain, wind, etc. Heavy metals are used in one of the most widespread treatments: CCA (Chrome, Copper, Arsenic).

CCA is a mixture of chrome, copper and arsenic. Each of those metals has its proper use: chrome as a fixing agent, copper as a fungicide and arsenic as an insecticide. Typically, a commercial CCA solution is composed of 34% chrome, 13% copper and 25% arsenic. The complement (28%) is water, which plays the role of solvent and carries preservative agents through the wood material. This concentrated solution is then highly diluted for the impregnation of wood. This chemical treatment can be easily recognized because of the green colour that it gives to the material due to the presence of copper.

CCA treatment can multiply the wood lifetime by 10. That is why, between 1975 and 1990, there was a rapid expansion of the use of CCA as a preservation agent for wood. This expansion was slowed down by the decision of some European countries to ban CCA due the toxicity of chrome and arsenic. However, each year 120 000 tonnes of CCA are still used all over the world to treat 20 millions m^3 of wood.

Because CCA treated wood has been classified as hazardous material, its disposal has become a great problem. Different alternatives have been proposed:

- The most convenient alternative for CCA treated wood waste could be landfill disposal. But this solution is limited by the number of waste disposal sites that decreases each year and by the problem of leached arsenic. Furthermore, since 2001 in Europe all wood wastes that have been treated with toxic substances are classified as hazardous materials. Consequently, in Europe landfill disposal of CCA treated wood waste is forbidden.
- Biological processes have also been proposed. But chrome and arsenic are usually toxic for micro-organisms. Consequently, whatever the conditions for the biological conversion (anaerobic or aerobic), the process is very slow or worst, does not proceed due to a high level of micro-organism death.
- Thermal conversion is another way for the disposal of waste wood. Combustion has the advantages of reducing the waste volume and of releasing heat that can be directly used. But burning CCA treated wood releases highly toxic gases due to the vaporization of heavy metals. A solution should be to send waste wood to incinerators equipped with gas cleaning system. But even at very low concentrations incinerators are usually not equipped to remove heavy metals from fumes before sending them to stacks.

* Corresponding author. Tel.: +33 559 407 809; fax: +33 559 407 801.
E-mail address: frederic.marias@univ-pau.fr (F. Marias).

0304-3894/$ – see front matter © 2009 Elsevier B.V. All rights reserved.
doi:10.1016/j.jhazmat.2009.05.077

Nomenclature

a, a_i	stoichiometric coefficients in pyrolysis model
a_w	water activity
A_i	Arrhenius pre-exponential factor of the chemical reaction i (s^{-1})
b	stoichiometric coefficient in pyrolysis model
C_p	specific heat at constant pressure (J/kg K)
D_b	diffusion coefficient of bound water (m^2/s)
D^i_{eff}	effective diffusivity of gaseous species i (m^2/s)
E_i	activation energy of the chemical reaction i (J/mol)
h	enthalpy (J/kg)
h°_f	standard formation enthalpy (J/kg)
k_i	kinetic constant of the chemical reaction i (s^{-1})
$h_{m(i)}$	Mass transfer coefficient for species i (m/s)
h_T	heat transfer coefficient (W/(m^2 K))
K_l	permeability of the liquid water phase (m^2)
K^l_r	relative permeability of the liquid water phase
K_g	permeability of the gas phase (m^2)
K^g_r	relative permeability of the gas phase
M	total moisture content
M_{FSP}	fibre saturation point
M_g	molecular weight of the gas phase (kg/mol)
M_i	molecular weight of the gaseous specie i (kg/mol)
n	unit normal vector
NGS	number of gaseous species
Nu	Nusselt number
R	particle radius (m)
Re	Reynolds number
R_i	rate of production of the gaseous species i (kg/m^3 s)
R_g	perfect gas constant (=8314 J/mol K)
P_c	capillary pressure (Pa)
$\langle P_l \rangle^l$	pressure in the liquid phase (Pa)
$\langle P_g \rangle^g$	pressure in the gas phase (Pa)
$P^{sat}_{H_2O(g)}$	vapour pressure of water (Pa)
Sc	Schmidt number
Sh	Sherwood number
t	time (s)
T, $\langle T \rangle$	temperature (K)
Tf	standard formation temperature (K)
v	velocity vector (m/s)

Subscripts

b	bound water phase
c	char phase
g	gas phase
inf	surrounding environment conditions
l	liquid or free water phase
surf	particle surface conditions
W	dried wood phase

Superscripts

b	bound water phase
c	char phase
g	gas phase
l	liquid or free water phase
W	dried wood phase

Greek letters

ΔH_{sorp}	heat of water sorption (J/kg K)
ε_α	volume fraction of the α phase
η	interpolation factor
μ	dynamic viscosity (Pa s)
$\langle \rho_\alpha \rangle$	mass concentration of the α phase inside the particle (kg/m^3)
τ	material tortuosity
υ_{ij}	stoichiometric coefficient of the specie i in the chemical reaction j
ψ_α	physical variable in the α phase
$\langle \psi_\alpha \rangle$	average of the physical variable ψ_α
$\langle \psi_\alpha \rangle^\alpha$	intrinsic average of the physical variable ψ_α

Furthermore, according to Duverneuil et al. [1], incineration of waste that contains high level of metals has to be avoided because it requires an auxiliary combustion, increasing operating costs. The best way to remove heavy metals from wood should be to keep them at their solid state and concentrate them. Slow pyrolysis is so suggested as a possible way.

Pyrolysis is a thermal degradation in absence of oxygen. Pyrolysis reactions lead to the production of three main fractions:

- a solid material, commonly named char,
- condensable gases at ambient conditions, referenced as tars,
- and permanent gases.

Depending upon the heating rate and the operating temperature, the yield of each fraction can be modified. In slow pyrolysis processes, char production is maximized, and in the specific context of CCA treated wood waste, slow pyrolysis conditions prevent the release of heavy metals from the solid waste by keeping them in the remaining solid matrix (char).

This mode of operation is the topic of this work. More precisely, our ultimate aim is to build a complete model for the Chartherm© reactor, developed by the Thermya company. The Chartherm© process, depicted in Fig. 1 (as proposed by Helsen [2]), can be decomposed in 3 main operations: a crushing step, a thermal degradation step and a refining step. The heart of the process is the reactor that is basically a counter current contactor where fresh particles of treated wood waste are fed by the top of a cylindrical reactor while hot gases (free of oxygen) are supplied at its bottom. During its transport from the top of the reactor to its bottom, a single particle of treated wood waste undergoes several phenomena such as heating, drying, pyrolysis and so on.

The mathematical modelling of the behaviour of a single particle undergoing slow pyrolysis is precisely the scope of this paper. In the first step of this modelling effort, the particle is supposed free of heavy metals.

Such a topic has already been developed in the literature. Bryden et al. [3], and Di Blasi [4] have written papers about modelling porous media undergoing pyrolysis. Di Blasi modelled a slab of wood convectively and radiatively heated. She studied the pyrolysis of a dry wooden slab in a one-dimensional problem. The model assumed that the studied sample volume did not change (no shrinkage) and that there was no diffusive transport of gases inside the particle. In their works, Bryden et al. [3] described the pyrolysis of a wooden slab heated by radiative transfer and took into account drying; which was modelled using an Arrhenius-type expression. No movement of water (convection, diffusion) was described in this model and there was no distinction between bound water and free water. Also, both Di Blasi [4] and Bryden et al. [3] did not take into account intra-particular diffusive transport through the porous media.

In the present work, because of the complex structure of wood and the complex nature of the equations describing transport in such a heterogeneous material, the choice has been made to use the

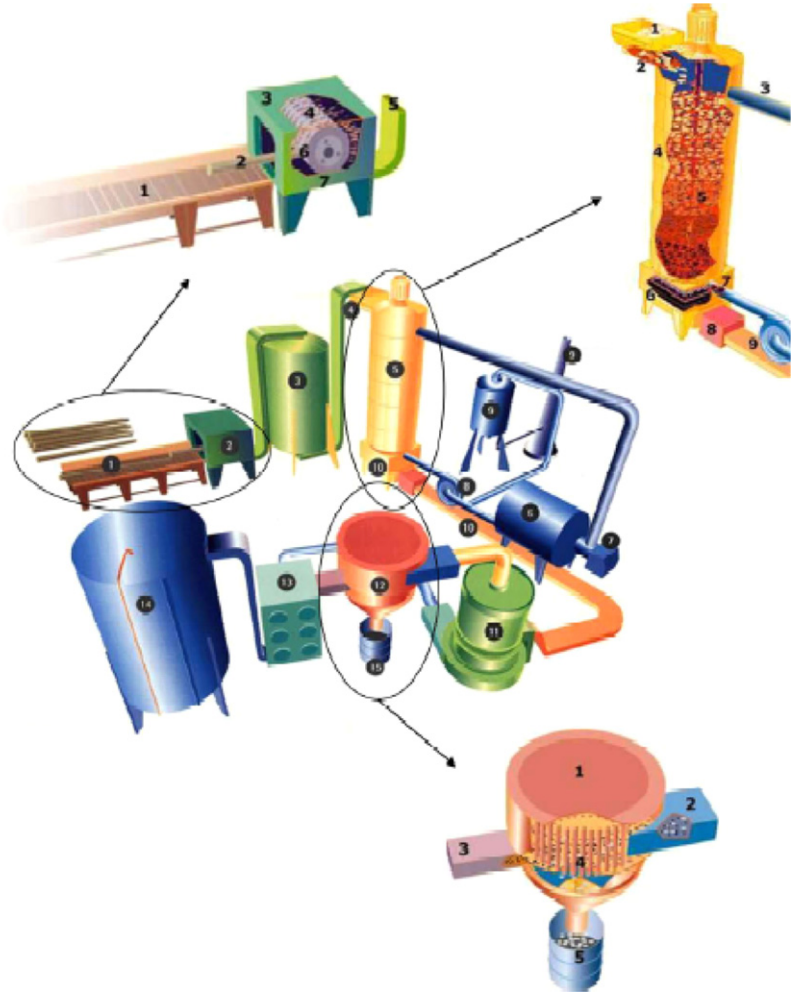

Fig. 1. Schematic presentation of the Chartherm process [2]. Global process: (1) chain conveyor, (2) crusher, (3) crushed wood silo, (4) feed hopper, (5) reactor, (6) hot gas generator, (7) afterburner, (8) compressor, (9) gas scrubber and chimney, (10) solid product extractor and conveyor, (11) mill, (12) pneumatic centrifugal separator, (13) carbon product collector, (14) carbon product storage, and (15) metal conditioning. Detail of crusher: (1) chain conveyor, (2) pole, (3) crusher, (4) inertia drum, (5) wood shred output, (6) wood crushing, and (7) metal scrap collector. Detail of reactor: (1) hopper, (2) crushed wood input, (3) gas output, (4) reactor, (5) crushed wood at different levels of charcherisation, (6) grate, (7) hot gas input, (8) carbon product extraction, and (9) carbon product output. Detail of separation: (1) pneumatic centrifugal separator, (2) carbon product input, (3) clean carbon output, (4) venting drum, and (5) heavy metals and minerals.

method of volume averaging [5]. This method is used to derive local volume-averaged equations that become valid everywhere inside the porous medium: the medium under consideration is "made homogeneous".

It is a very interesting concept because it allows the description of the porous medium as a continuum. The derivation of the mathematical model is the topic of the first part of this paper. Then, in a second part, some insights into the numerical procedure used to solve the model (partial differential equations) are given. Finally, some simulation results for one-dimensional transient problems in spherical coordinates with a single spherical particle of wood are presented. The influence of different parameters of the model is also investigated.

2. Description of the mathematical model

This section is devoted to the mathematical derivation of the model. Because drying and pyrolysis are important phenomena in the description of the behaviour of a single particle undergoing slow pyrolysis, we firstly give insights into these specific topics. Then, in the second part we present the general concept of the averaging method before entering the part devoted to the derivation of the balance equations.

2.1. Drying and pyrolysis

Initially, wood contains water in three forms: bound (adsorbed) water, liquid (free) water and water vapour. The first one is assumed to be hydrogen bounded to the complex constituents of wood; it interacts with the solid by sorption phenomena. Consequently, evaporation of bound water requires more energy than evaporation of free water. Liquid water is found in voids of the wood. As there is no hydrogen bonding, this water requires solely latent heat to evaporate.

Water vapour is in equilibrium with the two other forms of water. Thermodynamic equilibrium allows us to write for water vapour:

$$\langle P_{H_2O(g)}\rangle^g = a_w P^{sat}_{H_2O(g)} \quad (1)$$

where $\langle P_{H_2O(g)}\rangle^g$ is the partial pressure of water vapour, $P^{sat}_{H_2O(g)}$ is the saturated vapour pressure and a_w represents the activity of water, while the saturation vapour pressure solely depends upon temperature (Reid et al. [6]). An expression of the saturated vapour pressure can be found in Reid et al. [6]. Water activity depends on the value of the moisture content.

$$W_{(s)} \xrightarrow{k_1} G_{(g)} \quad 1$$
$$W_{(s)} \xrightarrow{k_2} T_{(g)} \quad 2$$
$$W_{(s)} \xrightarrow{k_3} C_{(s)} \quad 3$$

Fig. 2. Reaction scheme from Shafizadeh and Chin [8].

The total moisture content M is defined as the ratio of the sum of each concentration of water to the solid concentration:

$$M = \frac{\langle \rho_l \rangle + \langle \rho_b \rangle + \langle \rho_{H_2O(g)} \rangle}{\langle \rho_w \rangle} \quad (2)$$

where $\langle \rho_l \rangle$, $\langle \rho_b \rangle$ and $\langle \rho_{H_2O(g)} \rangle$ stand respectively for the concentration of liquid water, bound water and water vapour in the particle. $\langle \rho_w \rangle$ is the concentration of wood inside the particle.

The threshold moisture content from which wood contains only bound water is called the fibre saturation point M_{FSP}. If the initial moisture content is greater than M_{FSP}, wood contains liquid water. For most wood, the fibre saturation point is closed to 30%.

From this point, we can define the value of water activity. Indeed, if M is greater than M_{FSP}, the free water has the same physical properties as those of pure water and the activity is equal to 1. On the other hand, if M is lower than M_{FSP}, only bound water is present and its activity depends on the temperature and the moisture content (Grønli [7]):

$$a_w = 1 - \left(1 - \frac{M}{M_{FSP}}\right)^{0.00645T} \quad (3)$$

During drying, vaporization of free water requires energy: the latent heat of vaporization of water. Under the fibre saturation point value, vaporization of bound water occurs and it requires the latent heat of vaporization of water and an additional energy to desorb bound water from wood constituents: the energy of desorption.

When wet wood is heated, it first undergoes a drying period. Then, after this period, the temperature of the solid increases gradually and reaches a point at which the thermal decomposition takes place. This thermal decomposition is a complex process. As it was quoted in the introduction, pyrolysis produces gases, tar and char. To describe those reactions different models exist.

Shafizadeh and Chin [8] described wood thermal decomposition in three competitive reactions, which produce gas (G), tars (T) and char (C) (Fig. 2).

$k_i = A_i \exp(-E_i/(R_g T))$ stands for the reaction constant rate of the reaction i.

Regarding the Shafizadeh and Chin model, Thurner and Mann [9] provided kinetics data for first order reactions in the case of wood (Table 1).

Di Blasi [11] used Shafizadeh and Chin model for primary reactions and added secondary competitive reactions to describe tar cracking (Fig. 3). The corresponding kinetic parameters were also computed by Liden et al. [10] as it is shown in Table 1.

Those models are the simplest and most usual models that can be found in the literature. However, more complex kinetic models also exist. Indeed, Chan et al. [12] used Shafizadeh and Chin model and added a consecutive reaction which decomposes primary tars into lighter molecules (secondary gases ($G2$) and secondary tars ($T2$)) (Fig. 4). In this reaction pathway, a and b are stoichiometric coefficients that can be used to fit experimental results.

$$T_{(g)} \xrightarrow{k_4} G_{(g)} \quad 4$$
$$T_{(g)} \xrightarrow{k_5} C_{(s)} \quad 5$$

Fig. 3. Secondary reactions from Di Blasi [11].

$$W_{(s)} \xrightarrow{k_1} G_{1(g)} \quad 1$$
$$W_{(s)} \xrightarrow{k_2} T_{1(g)} \quad 2$$
$$W_{(s)} \xrightarrow{k_3} C_{(s)} \quad 3$$
$$T_{1(g)} \xrightarrow{k_4} aG_{2(g)} + bT_{2(g)} \quad 4$$

Fig. 4. Reaction scheme from Chan et al. [12].

$$W_{(s)} \xrightarrow{k_1} a_1 G_{1(g)} + (1-a_1) H_2O_{(v)} \quad 1$$
$$W_{(s)} \xrightarrow{k_2} T_{1(g)} \quad 2$$
$$W_{(s)} \xrightarrow{k_3} a_2 C + (1-a_2) H_2O_{(v)} \quad 3$$
$$T_{1(g)} \xrightarrow{k_4} a_3 G_{2(g)} + a_4 T_{2(g)} + (1-a_3-a_4) H_2O_{(v)} \quad 4$$
$$H_2O_{(b)} \xrightarrow{k_5} H_2O_{(v)} \quad 5$$

Fig. 5. Reaction scheme from Glaister [13].

Glaister [13] improved this model by taking into account water production as a primary tar component (Fig. 5). Indeed, from experiments, Chan et al. [12] and Hajaligol et al. [14] observed a production of water from 5 to 15% greater than the initial moisture content of wood. Each product is associated with a stoichiometric coefficient (a_1, a_2, a_3 or a_4) that can be used to fit experimental observation. The kinetic parameters of the model depicted by Glaister [13] are given in Table 2.

Concerning the framework of the present paper, the model of Shafizadeh and Chin [8] has been selected as it is commonly used for the description of thermal degradation of wood.

Regarding the composition of the permanent gases, Baumlin [15] showed that they were mainly composed of H_2, CH_4, CO, CO_2. The exact composition of these light gases is closely correlated with the operating conditions that drive the pyrolysis process itself. Baumlin [15] analysed the outlet gas flow rate from a CSTR where slow pyrolysis occurred. For wood pyrolysis at 540 °C, light gases are mostly composed of CO and CO_2. Low weight fractions are observed for H_2 and CH_4.

Concerning the compositions of tars, Reppelin [16] used a coupling TGA-FTIR to show that the tars were mainly composed of water, formic acid and acetic acid.

Table 1
Kinetic parameters for primary and secondary reactions.

Reaction	A [s^{-1}]	E [kJ/mol]	References
1	14,350	88.6	Measured by Thurner and Mann [9]
2	412,500	112.7	Measured by Thurner and Mann [9]
3	737,700	106.5	Measured by Thurner and Mann [9]
4	4,280,000	107.5	Measured by Liden et al. [10]
5	1,000,000	107.5	Estimated by Di Blasi [11]

Table 2
Kinetic parameters for Glaister model.

Reaction	A [s^{-1}]	E [kJ/mol]	a
1	1.3×10^8	140.3	0.7
2	2.0×10^8	133.1	0.9
3	1.1×10^7	121.4	0.65
4	1.5×10^6	114.3	0.25
5	4.0×10^2	25.1	–

Table 3
Species considered in the composition of gas (*G*) and tar (*T*).

Product	Formula
Nitrogen	N_2
Oxygen	O_2
Water	H_2O
Hydrogen	H_2
Methane	CH_4
Carbon oxide	CO
Carbon dioxide	CO_2
Formic acid	HCOOH
Acetic acid	CH_3COOH
Phenol	C_6H_5OH
Benzene	C_6H_6

These observations have led us to use the set of chemical species presented in Table 3 to build a model for describing the slow pyrolysis of wood.

2.2. Formulation of the problem

As it was seen previously, a particle of wood is a heterogeneous porous medium. Assuming the reaction scheme given in Section 2.1 (Shafizadeh and Chin [8] completed with kinetics data from Thurner and Mann [9]), it can be completely described as a mixture of five phases: dried wood (w), char (c), liquid water (l), bound water (b) and gaseous species (g) (see Fig. 6).

A method based on Whitaker's work on drying [5], called the method of volume averaging, allows us to derive local volume-averaged equations that are valid everywhere into the porous medium. Such a description requires preliminary definitions.

The average of a quantity ψ_α in the phase α over the volume V containing all the phases is defined as:

$$\langle\psi_\alpha\rangle = \frac{1}{V}\int_{V_\alpha}\psi_\alpha dV \tag{4}$$

where V_α is the volume occupied by the phase α in the averaging volume V.

The intrinsic phase average is also defined:

$$\langle\psi_\alpha\rangle^\alpha = \frac{1}{V_\alpha}\int_{V_\alpha}\psi_\alpha dV \tag{5}$$

The two definitions are linked together by:

$$\langle\psi_\alpha\rangle = \varepsilon_\alpha\langle\psi_\alpha\rangle^\alpha \tag{6}$$

where ε_α is the volume fraction of the phase α:

$$\varepsilon_\alpha = \frac{V_\alpha}{V} \tag{7}$$

The principle of the method allows us to consider the heterogeneous volume V as a new volume called Representative Elementary Volume (REV) which is a homogeneous multi-component volume (Fig. 6) and can be considered as a continuum.

2.3. Conservation equations

In this section, we present all the differential equations that are solved in our mathematical model. We also present some algebraic equations needed to solve the problem. All algebraic equations and all physical parameters are found in Appendix A.

2.3.1. Mass balance for the two solid phases

The two following equations result from the choice of the pyrolysis model of Shafizadeh and Chin [8]. In order to write mass conservation for the two 'solid' phases, we made the assumption of a non-deformable particle (no shrinkage). So, as the solid phases are fixed in the particle, the following averaged equations are derived:

$$\text{Wood}: \quad \frac{\partial\langle\rho_W\rangle}{\partial t} = -(\langle k_1\rangle + \langle k_2\rangle + \langle k_3\rangle)\langle\rho_W\rangle \tag{8}$$

$$\text{Char}: \quad \frac{\partial\langle\rho_c\rangle}{\partial t} = \langle k_3\rangle\langle\rho_W\rangle \tag{9}$$

where $\langle\rho_W\rangle$ and $\langle\rho_c\rangle$ represent respectively the concentration of wood and the concentration of char in the particle.

We also made the assumption that all the values $\langle k_i\rangle$ are calculated as follows, using the kinetic parameters provided by Thurner and Mann [9] (Table 1):

$$\langle k_i\rangle = A_i \exp\left(\frac{-E_i}{(Rg\langle T\rangle)}\right) \tag{10}$$

2.3.2. Mass balance in the gas phase

For any gaseous component i (except water vapour) in the gas phase, mass conservation can be written as follows:

$$\frac{\partial\langle\rho_i\rangle}{\partial t} + \nabla\cdot(\langle\rho_i\rangle^g\langle\mathbf{v}_g\rangle) = \langle R_i^{\text{heterogeneous}}\rangle + \langle R_i^{\text{homogeneous}}\rangle + \nabla\cdot\left\{\langle\rho_g\rangle^g\left[\varepsilon_g D_{eff}^i\cdot\nabla\left(\frac{\langle\rho_i\rangle^g}{\langle\rho_g\rangle^g}\right)\right]\right\} \tag{11}$$

where $\langle\rho_i\rangle$ represents the concentration of gaseous species i inside the particle, $\langle\mathbf{v_g}\rangle$ stands for the averaged velocity of the gas phase, ε_g is the volume fraction of the gas phase and D_{eff}^i is the effective diffusion coefficient of i in the gas mixture (see Appendix A).

$R_i^{\text{heterogeneous}}$ and $R_i^{\text{homogeneous}}$ represent respectively the rate of production of i by heterogeneous reaction and homogeneous reaction. These homogeneous reactions could be for example:

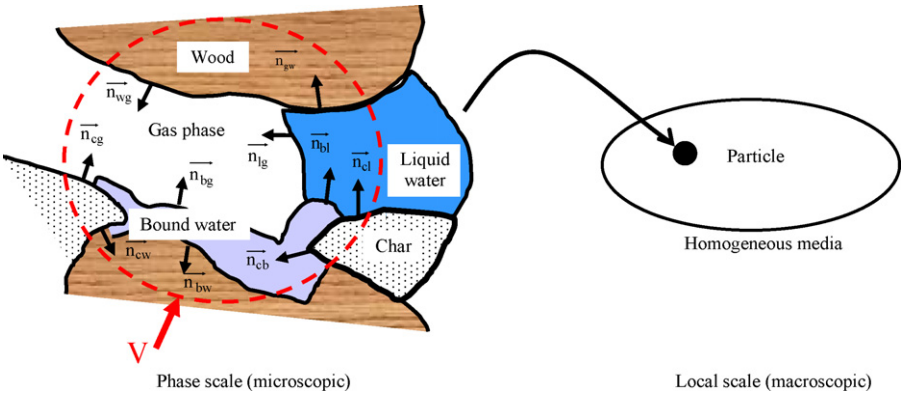

Fig. 6. Principle of homogenization by the method of the volume averaging.

Table 4
Composition of gas (G) and tar (T) used in the model.

Formula	Composition of gas (G)	Composition of tars (T)
N_2	–	–
O_2	–	–
H_2O	–	42 wt%
H_2	1 wt%	–
CH_4	1 wt%	–
CO	8 wt%	–
CO_2	90 wt%	–
HCOOH	–	10 wt%
CH_3COOH	–	28 wt%
C_6H_5OH	–	13 wt%
C_6H_6	–	7 wt%

- the water–gas shift reaction,
- the methane reforming reaction,
- the thermal cracking of tars in lighter molecules.

However, in the scope of this study we assume that these reactions do not have any important significance and hence we assume that all the $R_i^{\text{homogeneous}}$ are equal to zero.

Regarding the heterogeneous reactions, in the case of Shafizadeh and Chin model, $R_i^{\text{heterogeneous}}$ is computed as

$$\langle R_i^{\text{heterogeneous}} \rangle = \sum_{j=1}^{3} \upsilon_{ij} \langle k_j \rangle \langle \rho_W \rangle \tag{12}$$

where υ_{ij} is the stoichiometric coefficient of the species i in the reaction j. The values of these coefficients used in this work are summed up in Table 4, on a mass basis.

2.3.3. Mass balance for water

As it was quoted in the preceding paragraphs, intra-particular water exists in three different forms. For convenience's sake, it is easier to solve the mass balance equation for the total concentration of water (liquid + bound + vapour). The derivation of this one yields:

$$\frac{\partial(\langle \rho_l \rangle + \langle \rho_b \rangle + \langle \rho_{H_2O(g)} \rangle)}{\partial t} + \nabla \cdot (\langle \rho_l \rangle^l \langle \mathbf{v_l} \rangle) + \nabla \cdot (\langle \rho_b \mathbf{v_b} \rangle) + \nabla \cdot (\langle \rho_{H_2O(g)} \rangle^g \langle \mathbf{v}_g \rangle) - \nabla \cdot \left\{ \langle \rho_g \rangle^g \left[\varepsilon_g D_{eff}^{H_2O(g)} \cdot \nabla \left(\frac{\langle \rho_{H_2O(g)} \rangle^g}{\langle \rho_g \rangle^g} \right) \right] \right\} = \langle R_{H_2O(g)}^{\text{heterogeneous}} \rangle \tag{13}$$

$\langle \rho_l \rangle$, $\langle \rho_b \rangle$ and $\langle \rho_{H_2O(g)} \rangle$ are respectively the concentration of liquid water, the concentration of bound water and the concentration of water vapour in the particle, $\langle \mathbf{v_l} \rangle$ is the averaged velocity of the liquid water phase and $\mathbf{v_b}$ the velocity of the bound water phase.

2.3.4. Momentum balance

Darcy's law is used to compute the averaged velocity of the gas phase $\mathbf{v_g}$ and the averaged velocity of the liquid water $\mathbf{v_l}$:

$$\langle \mathbf{v_g} \rangle = -\frac{K_g K_r^g}{\mu_g} \nabla \langle P_g \rangle^g \tag{14}$$

$$\langle \mathbf{v_l} \rangle = -\frac{K_l K_r^l}{\mu_l} \nabla \langle P_l \rangle^l \tag{15}$$

where μ_g and μ_l stand respectively for the viscosity of the gas phase and the liquid water phase, K_g and K_l represent the intrinsic permeability of the gas phase and the liquid water phase, K_r^g and K_r^l are the relative permeability of the gas phase and the liquid water phase. The liquid pressure $\langle P_l \rangle^l$ is a function of the capillary pressure P_c and of the gas pressure $\langle P_g \rangle^g$:

$$\langle P_l \rangle^l = \langle P_g \rangle^g - P_c \tag{16}$$

Assuming that the equation of state of the gas is given by the ideal gas law, pressure $\langle P_g \rangle^g$ is linked to the local average temperature $\langle T \rangle$, to the total gas concentration $\langle \rho_g \rangle^g$ and to the molecular weight of the gaseous phase M_g:

$$\langle P_g \rangle^g = \frac{\langle \rho_g \rangle^g R_g \langle T \rangle}{M_g} \tag{17}$$

$$\langle \rho_g \rangle^g = \frac{1}{\varepsilon_g} \sum_{i}^{NGS} \langle \rho_i \rangle \tag{18}$$

2.3.5. Energy balance

In the porous particle, assuming all the phases have the same temperature and neglecting radiative heat transfer, the energy equation is derived as

$$\frac{\partial H}{\partial t} + \nabla \cdot \langle \rho_l \mathbf{v_l} \rangle \langle h_l \rangle^l + \nabla \cdot \langle \rho_b \mathbf{v_b} \rangle \langle h_b \rangle^b + \sum_{i}^{nc} \nabla \cdot \langle \rho_i \mathbf{v_l} \rangle \langle h_i \rangle^g = \nabla \cdot (\lambda_{eff} \nabla \langle T \rangle) \tag{19}$$

with the local total enthalpy:

$$H = \langle \rho_{BS} \rangle \langle h_{BS} \rangle^{BS} + \langle \rho_c \rangle \langle h_c \rangle^c + \langle \rho_l \rangle \langle h_l \rangle^l + \langle \rho_b \rangle \langle h_b \rangle^b + \sum_{i}^{nc} \langle \rho_i \rangle \langle h_i \rangle^g \tag{20}$$

where $\langle h_{BS} \rangle^{BS}$, $\langle h_c \rangle^c$, $\langle h_l \rangle^l$, $\langle h_b \rangle^b$ and $\langle h_i \rangle^g$ are respectively the enthalpy of wood, of char, of liquid water, of bound water, and of the gaseous species i.

λ_{eff} stands for the effective thermal conductivity, which is a combination of the thermal conductivity of each phase (see Appendix A).

In this work, we assume that enthalpy is independent of the condensed phase pressure. This assumption is also used for the determination of the enthalpy of the gases because of the assumption of ideal gas law.

Moreover, we also assume that the reference enthalpy for each phase is equal to the standard enthalpy of formation for the considered medium at the reference temperature:

$$h = h_f^\circ + \int_{Tf}^{T} CpdT \tag{21}$$

In the case of wood and char, the standard enthalpy of formation is computed using the lower heating values of these materials and their elemental composition (Boissonet and Seller [17]). More precisely, assuming theoretical combustion (with no air in excess), we can write the equation for the combustion of the material under study. Hence, given the fact that the standard enthalpy of this reaction is the exact opposite of the lower heating value and that we are able to compute the standard enthalpy of formation for the combustion products, it is possible to compute the standard enthalpy of formation of the wood (and of the char) by difference between the enthalpy of the products and the lower heating value. This also means that the heats of pyrolysis are included, by definition, in the standard enthalpy of formation of the material under consideration.

2.3.6. System/environment boundary conditions

Boundary conditions play a key role as they link the ambient surroundings and the considered particle together. In our case, the considered configuration is a spherical particle heated by a nitrogen convective flow. The ambient surroundings conditions are denoted using the subscript inf.

At the interface between the environment and our system, the mass and energy conservations, as well as the continuity of the mass flux and heat flux, have to be respected. Details relative to the derivation of these boundary conditions have been written by Erriguible [18].

For each gaseous species i, Eq. (11) and the following equation must be solved at any time at the external boundary of the particle:

$$\left(\langle\rho_i\rangle^g\langle\mathbf{v_g}\rangle - \langle\rho_g\rangle^g D^i_{eff}\cdot\nabla\left(\frac{\langle\rho_i\rangle}{\langle\rho_g\rangle}\right)\right)\cdot\mathbf{n} = h_{m(i)}(\langle\rho_i\rangle^g - \rho_{\inf(i)}) \tag{22}$$

where $h_{m(i)}$ stands for the external mass transfer coefficient of the gaseous species i.

Concerning water, Eq. (13) and the following equation must be solved at any time at the external boundary of the particle:

$$\left(\langle\rho_l\rangle^l\langle\mathbf{v_l}\rangle+\langle\rho_b\mathbf{v_b}\rangle+\langle\rho_{H_2O(g)}\rangle^g\langle\mathbf{v_g}\rangle-\langle\rho_g\rangle^g D^{H_2O(g)}_{eff}\cdot\nabla\left(\frac{\langle\rho_{H_2O(g)}\rangle}{\langle\rho_g\rangle}\right)\right)\cdot\mathbf{n} = h_{m(H_2O(g))}(\langle\rho_{H_2O(g)}\rangle^g - \rho_{\inf(H_2O(g))}) \tag{23}$$

The general expression of the continuity of the heat flux is given by

$$\left(\langle\rho_l\rangle^l\langle\mathbf{v_l}\rangle\langle h_l\rangle^l + \langle\rho_b\mathbf{v_b}\rangle\langle h_b\rangle^b + \sum_i\left(\langle\rho_i\rangle\langle\mathbf{v_g}\rangle^g - \langle\rho_g\rangle^g D^i_{eff}\cdot\nabla\left(\frac{\langle\rho_i\rangle}{\langle\rho_g\rangle}\right)\right)\langle h_i\rangle^g - \lambda eff\ \nabla\langle T\rangle\right)\cdot\mathbf{n} = h_T(\langle T\rangle - T_{\inf}) \tag{24}$$

where h_T represents the external heat transfer coefficient.

The continuity of pressure is directly given by the equality between the pressure at the surface of the particle and the external pressure $P_{\inf}$:

$$\langle P_g\rangle^g = P_{\inf} \tag{25}$$

2.4. State variables

Here are given the variables that are computed by the model, the associated equations and the boundary conditions.

Variable	Equation
Concentration of wood: $\langle\rho_W\rangle$	Mass conservation: $\forall r$ and $\forall t$ $\quad\frac{\partial\langle\rho_W\rangle}{\partial t} = -(\langle k_1\rangle+\langle k_2\rangle+\langle k_3\rangle)\langle\rho_W\rangle$
Concentration of char: $\langle\rho_c\rangle$	Mass conservation: $\forall r$ and $\forall t$ $\quad\frac{\partial\langle\rho_C\rangle}{\partial t} = \langle k_3\rangle\langle\rho_W\rangle$
Total concentration of water: $\langle\rho_l\rangle+\langle\rho_b\rangle+\langle\rho_{H_2O(g)}\rangle$	Mass conservation: for $r=0$ and $\forall t$ $\quad\left.\frac{\partial(\langle\rho_l\rangle+\langle\rho_b\rangle+\langle\rho_{H_2O(g)}\rangle)}{\partial r}\right\|_{t,0} = 0$ for $r\#0$, $r\#R$ and $\forall t$ $\quad\frac{\partial(\langle\rho_l\rangle+\langle\rho_b\rangle+\langle\rho_{H_2O(g)}\rangle)}{\partial t}+\nabla\cdot(\langle\rho_l\rangle^l\langle\mathbf{v_l}\rangle)+\nabla\cdot(\langle\rho_b\mathbf{v_b}\rangle)+\nabla\cdot(\langle\rho_{H_2O(g)}\rangle^g\langle\mathbf{v_g}\rangle)-\nabla\cdot\left\{\langle\rho_g\rangle^g\left[\varepsilon_g D^{H_2O(g)}_{eff}\cdot\nabla\left(\frac{\langle\rho_{H_2O(g)}\rangle^g}{\langle\rho_g\rangle^g}\right)\right]\right\} = \langle R^{heterogeneous}_{H_2O(g)}\rangle$ for $r=R$ and $\forall t$ $\quad\frac{\partial(\langle\rho_l\rangle+\langle\rho_b\rangle+\langle\rho_{H_2O(g)}\rangle)}{\partial t}+\nabla\cdot(\langle\rho_l\rangle^l\langle\mathbf{v_l}\rangle)+\nabla\cdot(\langle\rho_b\mathbf{v_b}\rangle)+\nabla\cdot(\langle\rho_{H_2O(g)}\rangle^g\langle\mathbf{v_g}\rangle)-\nabla\cdot\left\{\langle\rho_g\rangle^g\left[\varepsilon_g D^{H_2O(g)}_{eff}\cdot\nabla\left(\frac{\langle\rho_{H_2O(g)}\rangle^g}{\langle\rho_g\rangle^g}\right)\right]\right\} = \langle R^{heterogeneous}_{H_2O(g)}\rangle\left(\langle\rho_l\rangle^l\langle\mathbf{v_l}\rangle+\langle\rho_b\mathbf{v_b}\rangle+\langle\rho_{H_2O(g)}\rangle^g\langle\mathbf{v_g}\rangle-\langle\rho_g\rangle^g D^{H_2O(g)}_{eff}\cdot\nabla\left(\frac{\langle\rho_{H_2O(g)}\rangle}{\langle\rho_g\rangle}\right)\right)\cdot\mathbf{n} = h_{m(H_2O(g))}(\langle\rho_{H_2O(g)}\rangle^g - \rho_{\inf(H_2O(g))})$
Concentration of water vapour: $\langle\rho_{H_2O(g)}\rangle$	Thermodynamical equilibrium: $\forall r$ and $\forall t$ $\quad\langle\rho_{H_2O(g)}\rangle = f(M,\langle T\rangle)$ (see Appendix A)
Porosity: ε_g	$\forall r$ and $\forall t$ $\quad\varepsilon_g = 1-\left(\frac{\langle\rho_W\rangle}{\langle\rho_W\rangle^W}+\frac{\langle\rho_C\rangle}{\langle\rho_C\rangle^c}+\frac{\langle\rho_l\rangle}{\langle\rho_l\rangle^l}+\frac{\langle\rho_b\rangle}{\langle\rho_b\rangle^b}\right)$
Concentration of gaseous species i (except water): $\langle\rho_i\rangle$	Mass conservation: for $r=0$ and $\forall t$ $\quad\left.\frac{\partial\langle\rho_i\rangle}{\partial r}\right\|_{t,0} = 0$ for $r\#0$, $r\#R$ and $\forall t$ $\quad\frac{\partial\langle\rho_i\rangle}{\partial t}+\nabla\cdot(\langle\rho_i\rangle^g\langle\mathbf{v_g}\rangle) = \langle R^{heterogeneous}_i\rangle+\nabla\cdot\left\{\langle\rho_g\rangle^g\left[\varepsilon_g D^i_{eff}\cdot\nabla\left(\frac{\langle\rho_i\rangle^g}{\langle\rho_g\rangle^g}\right)\right]\right\}$ for $r=R$ and $\forall t$ $\quad\frac{\partial\langle\rho_i\rangle}{\partial t}+\nabla\cdot(\langle\rho_i\rangle^g\langle\mathbf{v_g}\rangle) = \langle R^{heterogeneous}_i\rangle+\nabla\cdot\left\{\langle\rho_g\rangle^g\left[\varepsilon_g D^i_{eff}\cdot\nabla\left(\frac{\langle\rho_i\rangle^g}{\langle\rho_g\rangle^g}\right)\right]\right\}\left(\langle\rho_i\rangle^g\langle\mathbf{v_g}\rangle-\langle\rho_g\rangle^g D^{i(g)}_{eff}\cdot\nabla\left(\frac{\langle\rho_{i(g)}\rangle}{\langle\rho_g\rangle}\right)\right)\cdot\mathbf{n} = h_{m(i)}(\langle\rho_i\rangle^g-\rho_{\inf(H_2O(g))})$
Total gas concentration in the gas phase: $\langle\rho_g\rangle^g$	Summation: $\forall r$ and $\forall t$ $\quad\langle\rho_g\rangle^g = \frac{1}{\varepsilon_g}\sum_i^{NGS}\langle\rho_i\rangle$
Energy: H	Energy conservation: for $r=0$ and $\forall t$ $\quad\left.\frac{\partial H}{\partial r}\right\|_{t,0} = 0$ for $r\#0$, $r\#R$ and $\forall t$ $\quad\frac{\partial H}{\partial t}+\nabla\cdot\langle\rho_l\mathbf{v_l}\rangle\langle h_l\rangle^l+\nabla\cdot\langle\rho_b\mathbf{v_b}\rangle\langle h_b\rangle^b+\sum_i^{nc}\nabla\cdot\langle\rho_i\mathbf{v_i}\rangle\langle h_i\rangle^g = \nabla\cdot(\lambda_{eff}\nabla\langle T\rangle)$ for $r=R$ and $\forall t$ $\quad\frac{\partial H}{\partial t}+\nabla\cdot\langle\rho_l\mathbf{v_l}\rangle\langle h_l\rangle^l+\nabla\cdot\langle\rho_b\mathbf{v_b}\rangle\langle h_b\rangle^b+\sum_i^{nc}\nabla\cdot\langle\rho_i\mathbf{v_i}\rangle\langle h_i\rangle^g =$ $\nabla\cdot(\lambda_{eff}\nabla\langle T\rangle)\left(\langle\rho_l\rangle^l\langle\mathbf{v_l}\rangle\langle h_l\rangle^l+\langle\rho_b\mathbf{v_b}\rangle\langle h_b\rangle^b+\sum_i\left(\langle\rho_i\rangle\langle\mathbf{v_g}\rangle^g-\langle\rho_g\rangle^g D^i_{eff}\cdot\nabla\left(\frac{\langle\rho_i\rangle}{\langle\rho_g\rangle}\right)\right)\langle h_i\rangle^g-\lambda eff\ \nabla\langle T\rangle\right)\cdot\mathbf{n} = h_T(\langle T\rangle-T_{\inf})$
Temperature: $\langle T\rangle$	$\forall r$ and $\forall t$ $\quad H = \langle\rho_{BS}\rangle\langle h_{BS}\rangle^{BS}+\langle\rho_c\rangle\langle h_c\rangle^c+\langle\rho_l\rangle\langle h_l\rangle^l+\langle\rho_b\rangle\langle h_b\rangle^b+\sum_i^{nc}\langle\rho_i\rangle\langle h_i\rangle^g$
Gas pressure: $\langle\rho_g\rangle^g$	for $r\#R$ and $\forall t$ $\quad\langle P_g\rangle^g = \frac{\langle\rho_g\rangle^g R_g\langle T\rangle}{M_g}$ for $r=R$ and $\forall t$ $\quad\langle P_g\rangle^g = P_{\inf}$

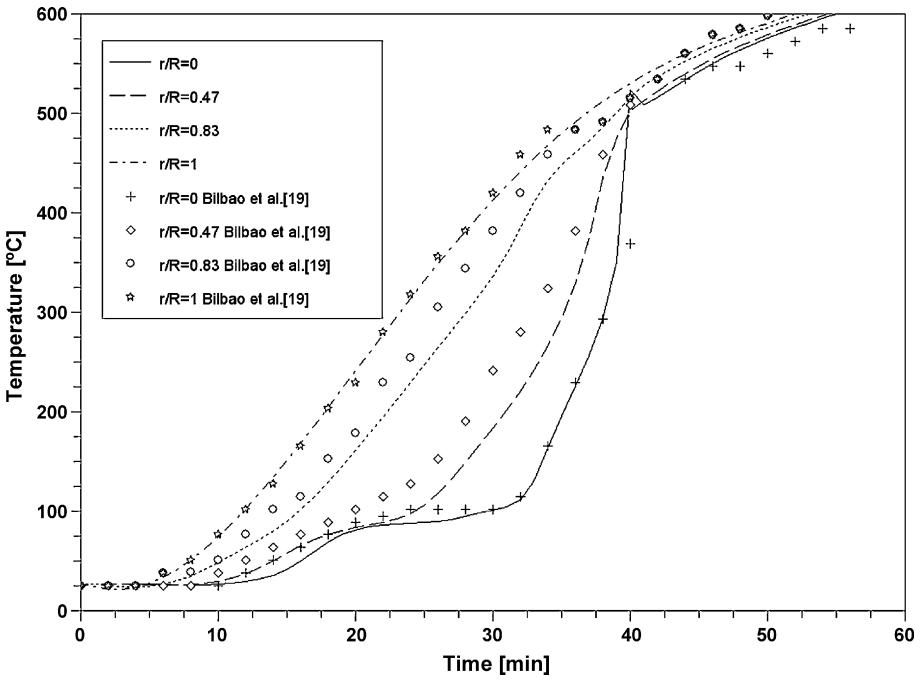

Fig. 7. Comparison between the experimental results of Bilbao et al. [18] and the numerical prediction of the model.

2.5. Numerical procedure

The mathematical model is a set of partial differential equations and algebraic equations. The numerical resolution of this system requires a preliminary operation of discretization (time or/and spatial). Several methods exist for the discretization of such a system. In our work, it has been chosen to use the method of lines. This means that first the system is spatially discretized (using finite differences), resulting in a set of ordinary differential equations and algebraic equations. We can write this set in the form of

$$\Phi(U,t)\frac{dU}{dt} = f(U,t)$$

where U represents the vector of all the state variables of the system, t is the time (variable of integration) and Φ is a matrix whose coefficients depends upon time and U. Gear's method was used to solve this system. This method requires the evaluation of the Jacobian of the system which was computed analytically.

3. Results and discussion

The equations are solved for one-dimensional transient problems in spherical coordinates. The variables depend only on time and on the radial position r inside the particle. In the following

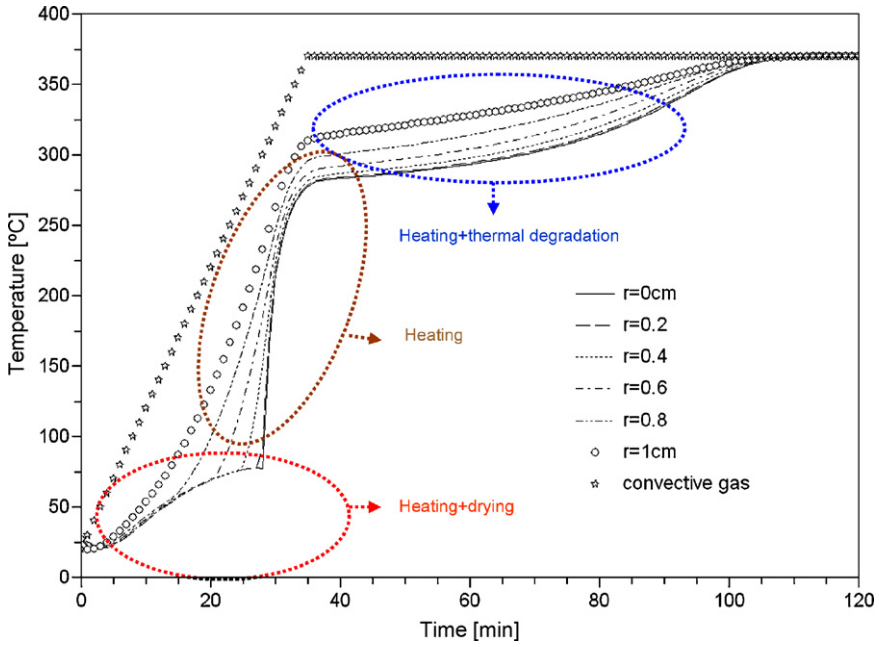

Fig. 8. Transient evolution of temperature during the overall process.

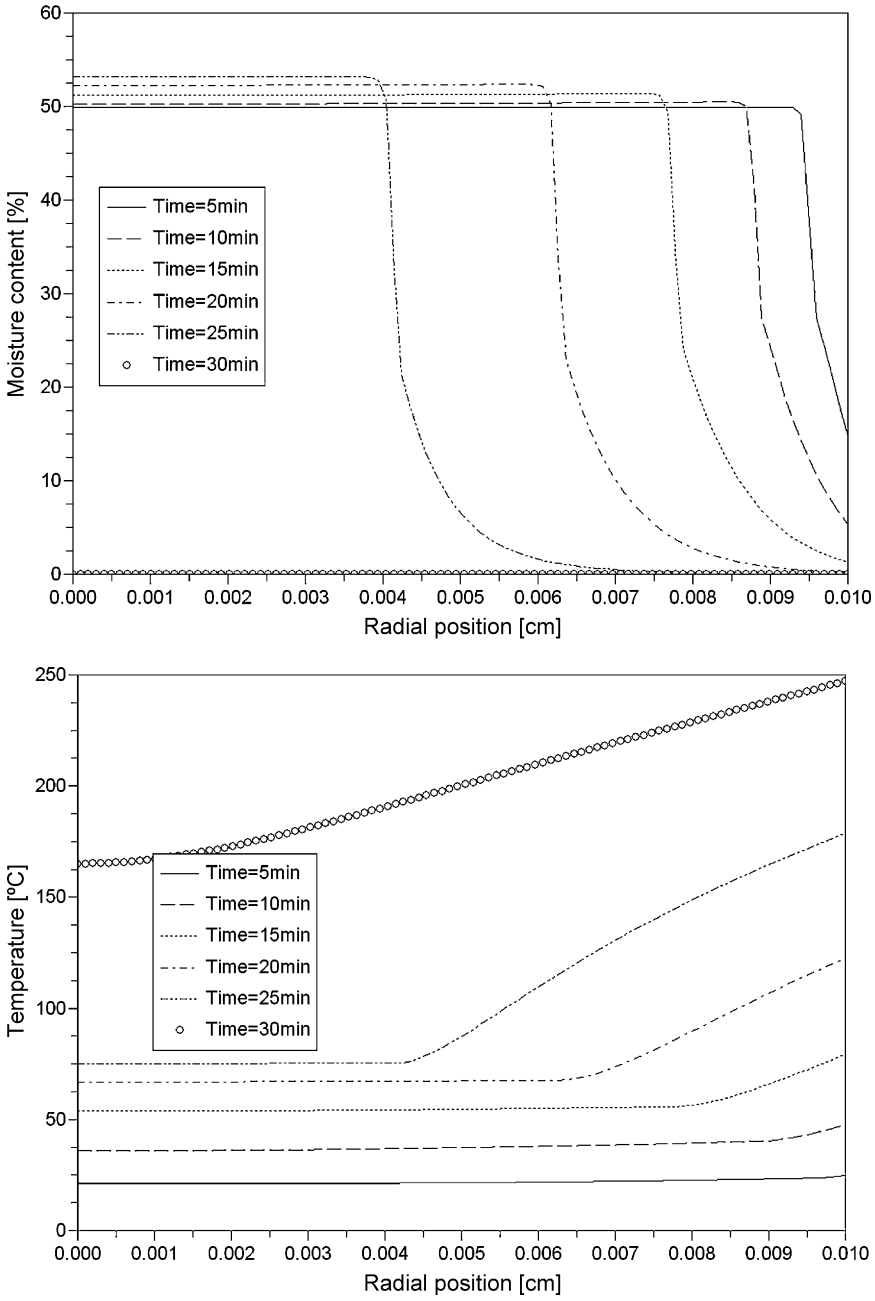

Fig. 9. Internal profiles of moisture content and temperature during drying.

results, it should be noticed that the computations were done using 100 nodes for the spatial discretization.

3.1. Validation

In order to validate the model, the choice has been made to use the experiments of Bilbao et al. [19]. They studied the pyrolysis of large spherical particles (2–5.6 cm in diameter) of pine and measured the temperature at different points inside the solid. Their experimental system is a cylindrical reactor of 8 cm internal diameter electrically heated by a furnace where nitrogen is used as an inert gas (flow rate 15 cm^3/s). Most of their results were obtained for a particle diameter of 5.6 cm, and a heating rate of 12 °C/min.

Fig. 7 gives a representation of the evolution of the temperature inside the material as measured by Bilbao et al. [19] together with the numerical prediction of our model. As it can be seen, the numerical prediction fits particularly well the experimental results, what we consider as a good validation of our model.

3.2. Description of the system under study

In the frame of this study, the choice has been made to consider a flow rate of nitrogen, whose initial superficial velocity is 1 $m\,s^{-1}$. The temperature of the carrier gas increases at a rate of 10 °C/min from 25 °C to 370 °C and its pressure is equal to the atmospheric pressure. The particle under investigation is a spherical particle of 1 cm diameter with an initial moisture content of 50%. Fig. 8 represents the transient evolution of the temperature at different positions inside the particle. At a glance, it clearly shows three main steps: drying, heating and pyrolysis.

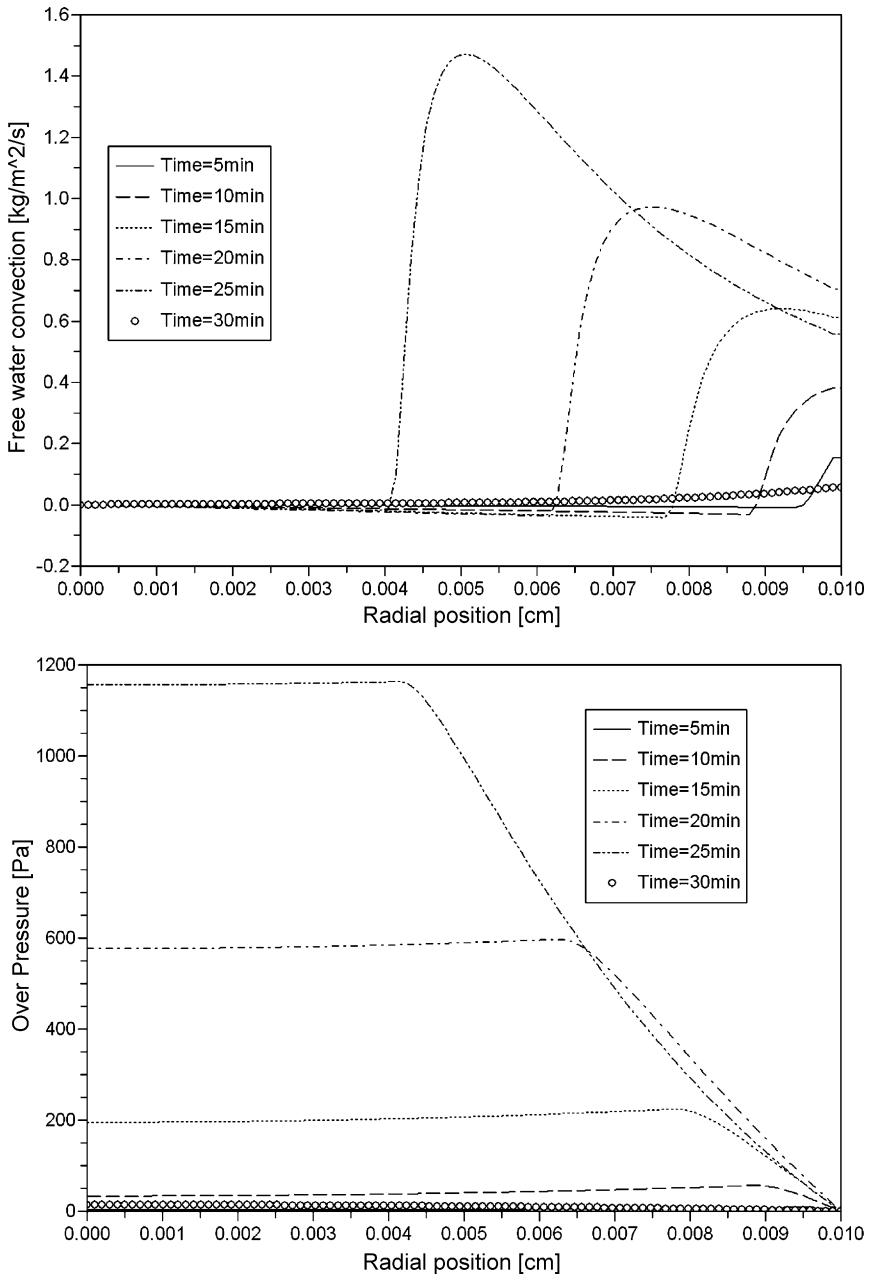

Fig. 10. Internal profiles of free water convection and gas overpressure during drying.

3.3. Drying

The results for the drying step are shown in Figs. 9–13. Regarding Figs. 8–10, one is able to give a precise estimation of the time required for the drying of the whole particle. Indeed, Fig. 8 clearly shows that for this particular time the temperature raises at the centre of the particle. Fig. 9 also shows that the profile of content collapses between 25 min and 30 min, and that the temperature inside the material increases suddenly once the drying is completed.

At the beginning of the process, convective gas does not bring enough energy to ensure vaporization of water. Indeed, drying requires energy to evaporate water and to release bound water. Because of this imbalance, energy is taken from the particle itself, what results in the decrease of its own temperature (its initial temperature was 25 °C whereas it is 20 °C after 5 min, Fig. 9). Drying proceeds progressively from the external surface ($r = 1$ cm) of the particle to its centre ($r = 0$ cm). This can be seen in Fig. 9 where it should also be noticed that the local temperature begins to raise once the corresponding moisture content has collapsed. Therefore, the difference between the temperature of the surface and the temperature of the centre raises as drying proceeds.

One can also observe in Fig. 9 an increase in the moisture content at the centre of the particle compared to the initial value (50%, on a raw basis). This can be explained with Fig. 10. On this figure, the free water convection flux ($\langle \rho_l \rangle^l \langle \mathbf{v_l} \rangle$) in Eq. (13) is plotted against radial position inside the particle and for different times. Also the gas overpressure is represented at different positions and for different times. The analysis of this figure shows that as the drying front line moves from the external limit of the particle to its centre an important overpressure appears in the gas phase (which results from the evaporation of liquid water). As it could be expected, a

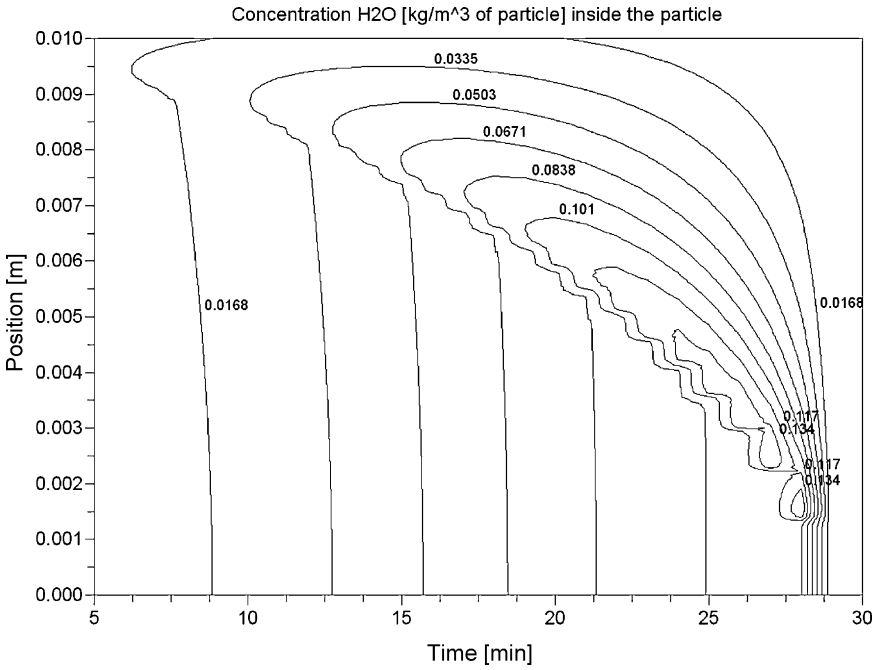

Fig. 11. Internal and transient profile of H_2O vapour concentration during the overall process.

gradient of pressure comes with this local overpressure. This gradient is negative towards the external surface of the particle, what in turns leads to a positive value for the free water convection flux. Free water is driven towards the external part of the particle and drying proceeds along "an expected route". However, it can be also observed that this overpressure is responsible for a positive gradient of pressure towards the centre of the particle This leads to negative values for the free water convection flux (Fig. 11) and thus to an accumulation of free water at the centre of the particle (Fig. 9).

To conclude with the drying step, Figs. 11 and 12 shows respectively the water vapour concentration in the gas phase and the overpressure in the gas phase during the overall process (drying and pyrolysis). These figures clearly indicate that the gaseous water yield is mainly due to the drying step and that this corresponds to the highest overpressures. In other words, this means that drying exerts higher constraints on the material than pyrolysis does.

3.4. Thermal degradation

Given the kinetics data provided by Thurner and Mann [9], and using the profile of temperature, wood composition and char composition depicted in Figs. 13 and 14, it can be observed that the thermal degradation starts 35 min after the beginning of the process and lasts until 117 min. As it was also mentioned in the

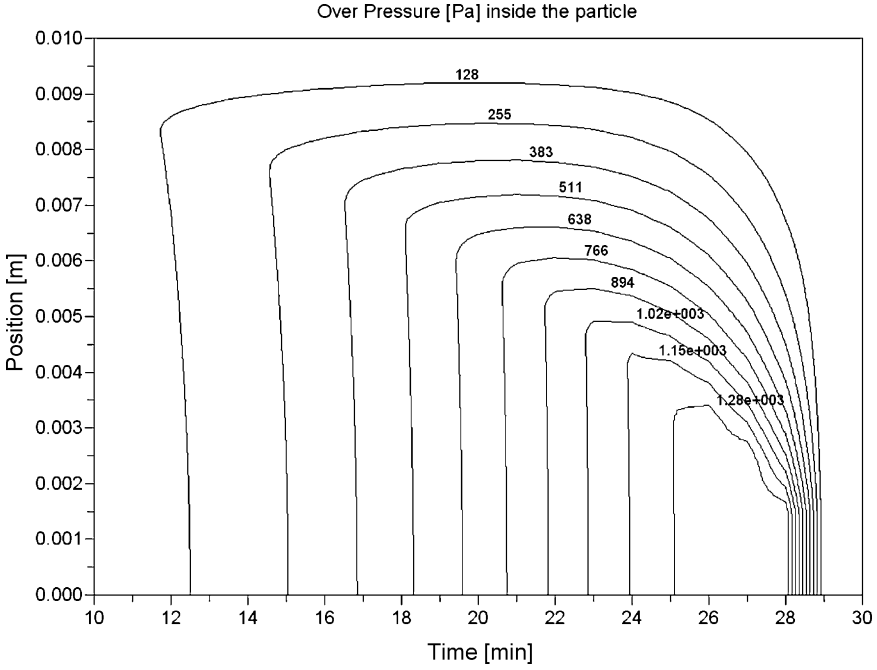

Fig. 12. Internal and transient profile of gas overpressure during the overall process.

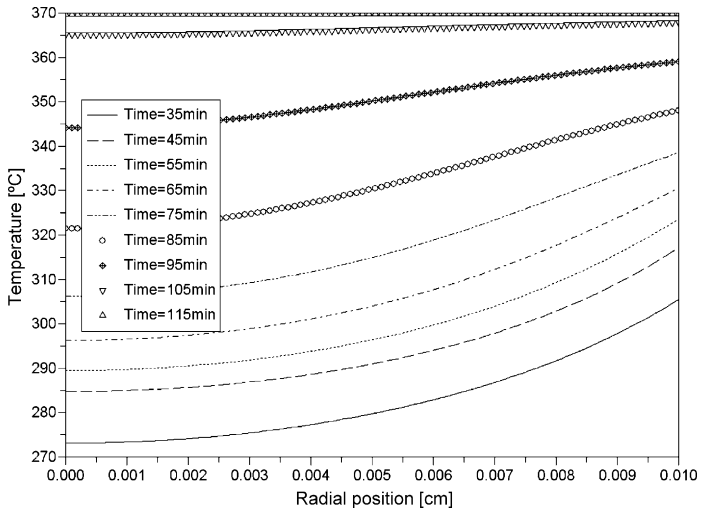

Fig. 13. Internal profiles of temperature during pyrolysis.

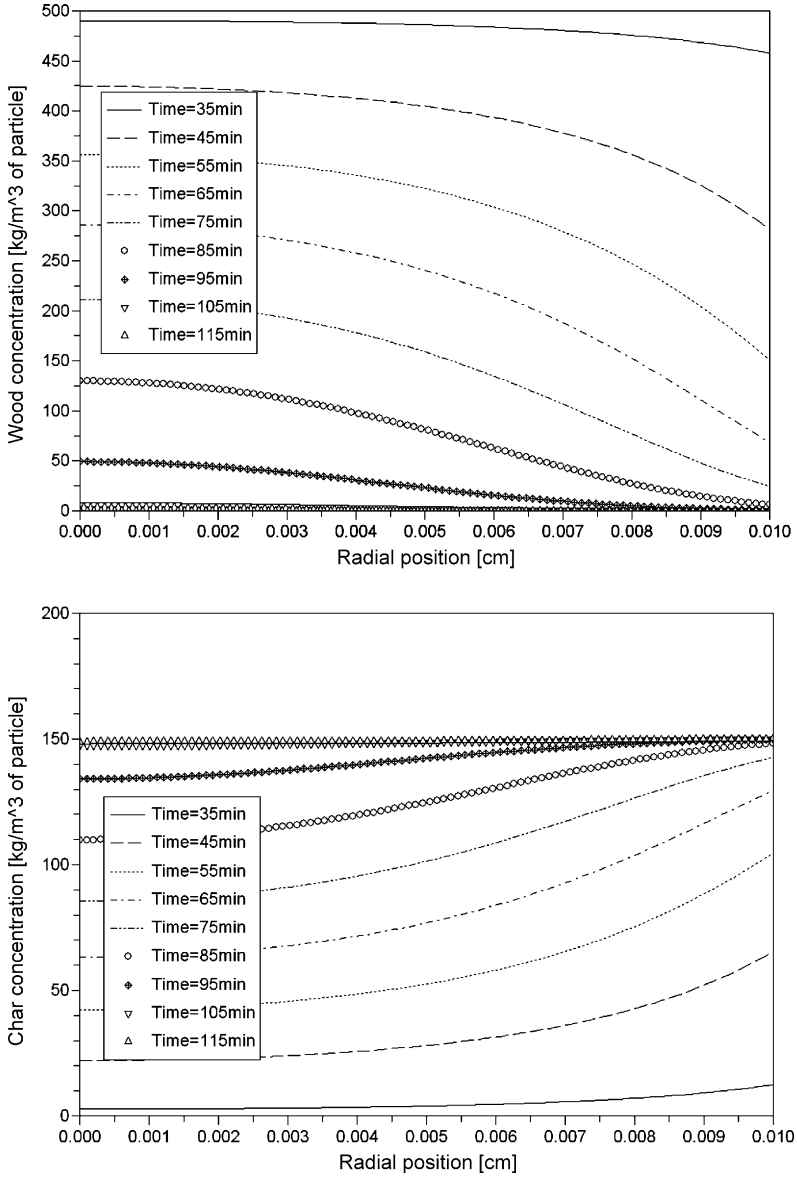

Fig. 14. Internal profiles of wood and char concentration during pyrolysis.

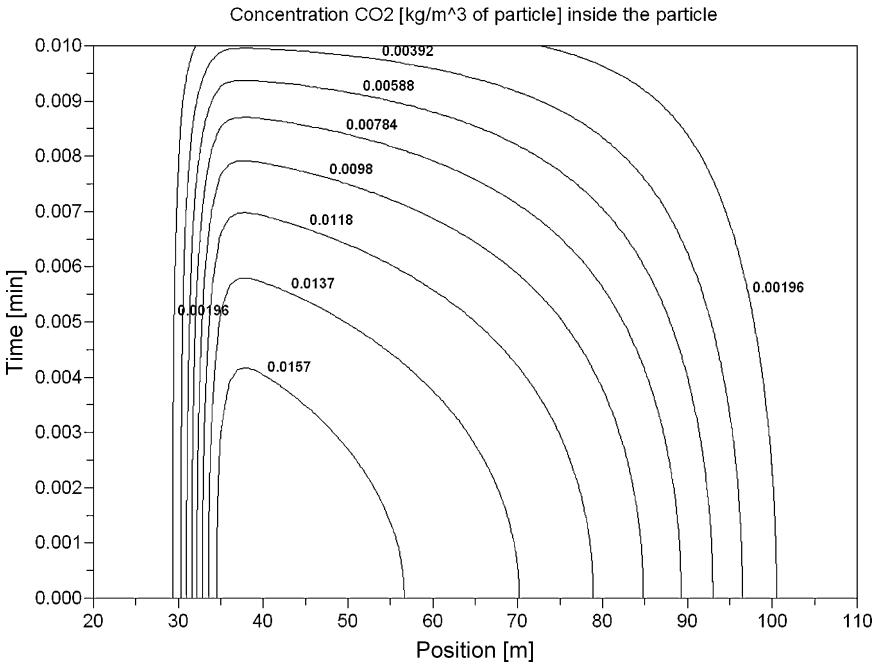

Fig. 15. Internal and transient profile of CO_2 vapour concentration during the overall process.

Table 5
Directional parameters used in our simulations.

	Radial direction	Tangential direction
Wood conductivity	0.15 [W/(m K)]	0.35 [W/(m K)]
Relative permeability for free water phase	$K_r^l = \left(\frac{M_l}{M_{lsat}}\right)^3$	$K_r^l = \left(\frac{M_l}{M_{lsat}}\right)^8$
Permeability for free water phase	5×10^{-16} [m^2]	5×10^{-13} [m^2]
Relative permeability for gas phase	$K_r^g = 1 + \left(2\frac{M_l}{M_{lsat}} - 3\right)\left(\frac{M_l}{M_{lsat}}\right)^2$	$K_r^g = 1 + \left(4\frac{M_l}{M_{lsat}} - 5\right)\left(\frac{M_l}{M_{lsat}}\right)^4$
Permeability for gas phase	$K_g = \eta \times 5 \times 10^{-16} + (1-\eta) \times 10^{-10}$ [m^2]	$K_g = \eta \times 5 \times 10^{-13} + (1-\eta) \times 10^{-10}$ [m^2]
Diffusion coefficient for bound water	$D_b = \exp\left(-9.9 + 9.8 \times M_b - \frac{4300}{T}\right)$ [m^2/s]	$D_b = 2.5\exp\left(-9.9 + 9.8 \times M_b - \frac{4300}{T}\right)$ [m^2/s]

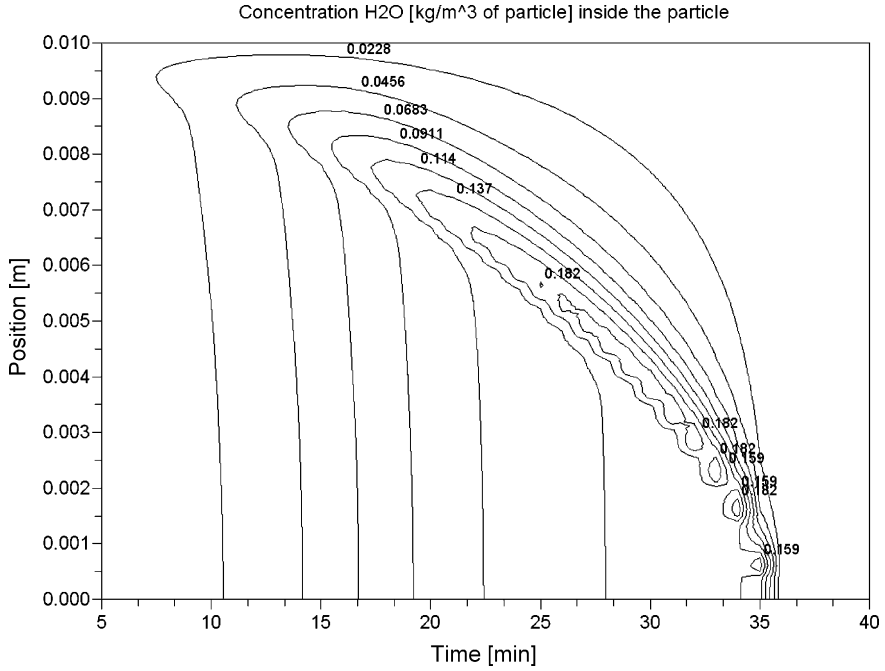

Fig. 16. Internal and transient profile of H_2O vapour concentration during the overall process (radial).

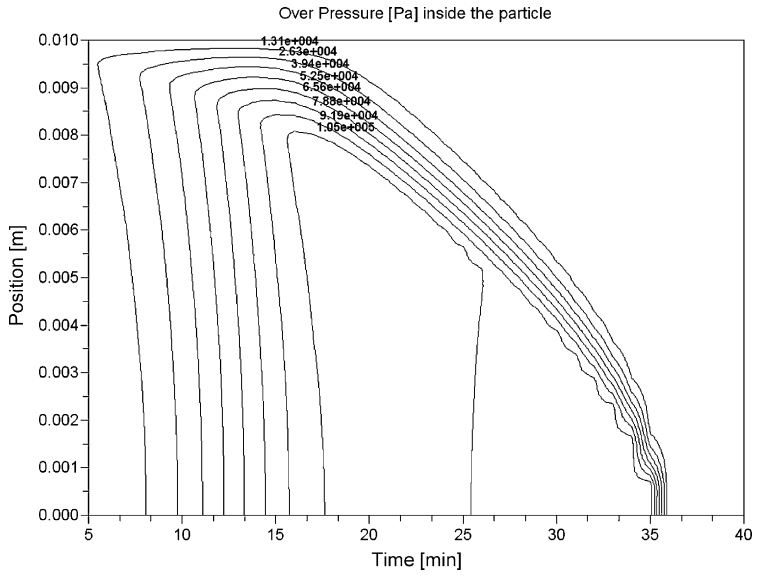

Fig. 17. Internal and transient profile of gas overpressure during the overall process (radial).

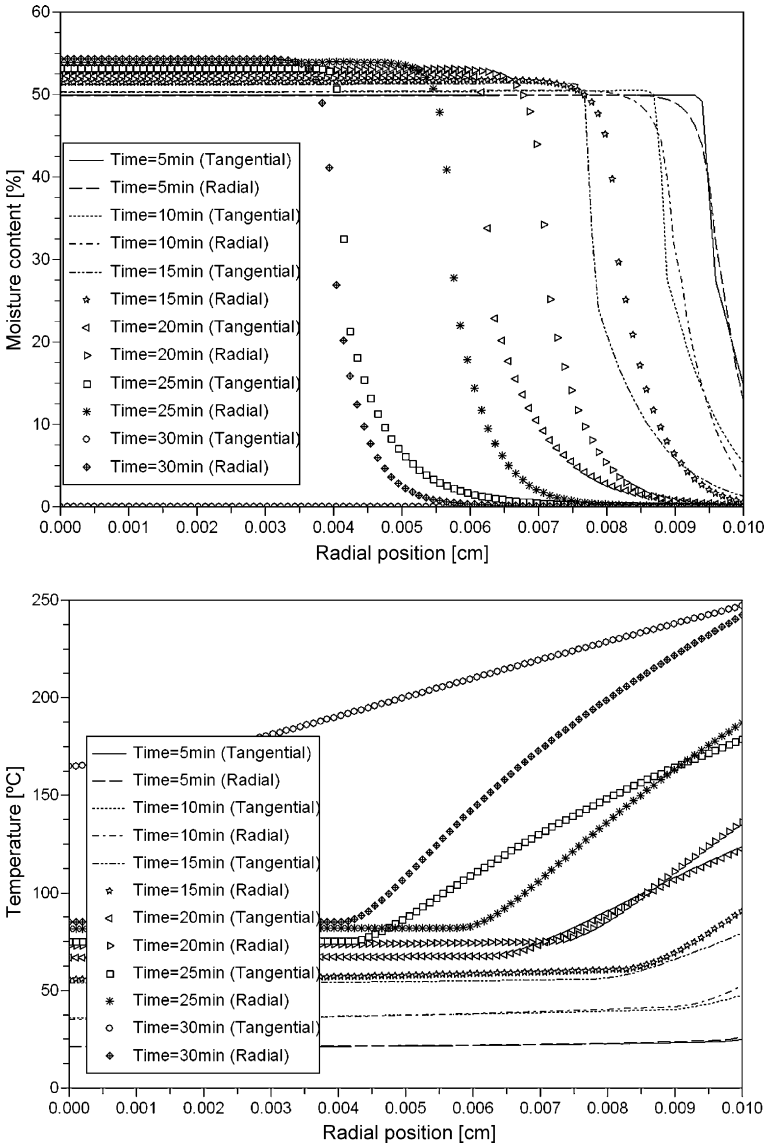

Fig. 18. Influence of transport properties (radial–tangential) on the internal profiles of moisture content and temperature during drying.

preceding paragraph, the pyrolysis step seems to operate softly compared to the drying step. Indeed, internal gradients of temperature and solid concentrations (wood, char) are low, whereas the profiles of temperature and moisture content exhibit sharp variations during the drying period. As pyrolysis proceeds, dry wood is converted into char from the external surface of the particle (where the temperature is higher) towards its centre. This conversion of wood not only leads to the production of char but also to the production of gases and tar, according to the reaction pathway that was used in this study (Shafizadeh and Chin [8]). As an illustration of this gas yield, Fig. 15 shows the evolution of carbon dioxide within the particle. Once the pyrolysis step has begun, there is a sharp increase in the concentration of carbon dioxide within the whole particle. Its production is higher than its external transfer to the surroundings. This leads to an accumulation of this species inside the particle at the very beginning of the pyrolysis step. However, because, it is transferred to the surroundings; the internal concentration of this species is higher near the centre of the particle than it is near its external surface. Regarding this figure, it can also be concluded that the release of the gaseous carbon dioxide from the particle to the surroundings seems to be faster than its production once the pyrolysis has begun. Indeed, the highest concentration at the centre begins to decrease at the quasi-beginning of this period, whereas the pyrolysis step still proceeds.

3.5. Influence of the numerical parameters

As it can be seen in Appendix A of this paper, the solving of the model presented in this work requires a lot of numerical parameters. Concerning slow pyrolysis of wood, an important parameter is the thermal conductivity because the overall conversion process (drying-pyrolysis) is mainly driven by heat transfer within the particle itself. Other important parameters are the permeabilities

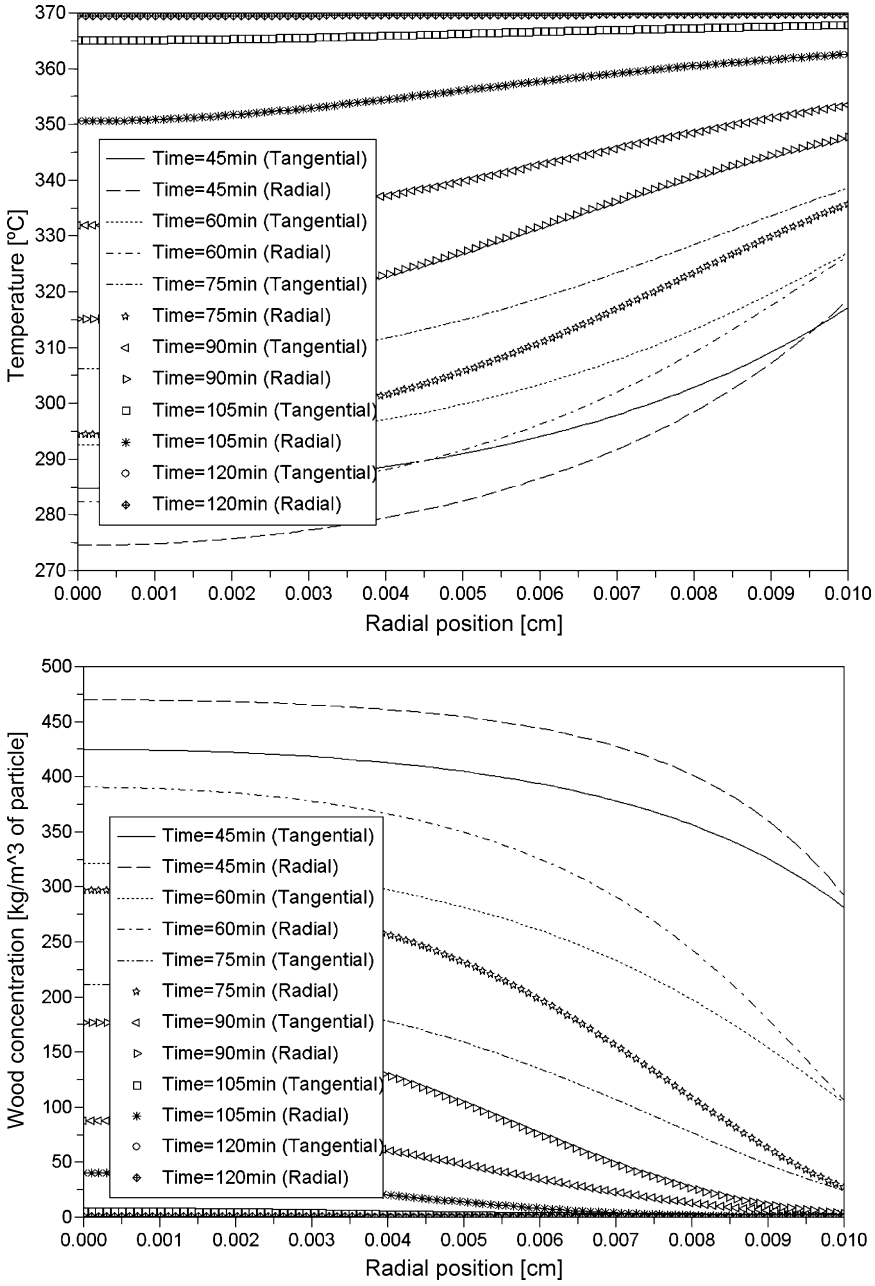

Fig. 19. Influence of transport properties (radial–tangential) on the internal profiles of temperature and wood concentration during drying.

because they impose the intensity of internal transfers of matter. These parameters are all the more important since wood is not an isotropic material. Indeed, its physical properties can be different whether transfer is considered perpendicularly to the wood fibres (radial transfer) or parallel to these fibres (tangential transfer).

The results that were presented in the preceding sections were obtained using the "tangential properties". In this configuration, transfers have higher intensities than they would have using "radial properties", what results in shorter times for both drying and pyrolysis. The study of the influence of these properties is the scope of this section. For that, computations are performed using the same operating parameters than in the preceding section, but with "radial properties" (see Table 5 and Appendix A for details).

Figs. 16 and 17 shows respectively the evolution of water vapour concentration in the particle and the gas overpressure in the case of "radial properties". These figures have to be compared to Figs. 11 and 12, which show the same data in the case of "tangential properties". Because transport of water vapour is more difficult in the case of "radial properties" (this can be observed by the higher water vapour concentration: 0.15 kg m^{-3} for tangential, 0.19 kg m^{-3} for radial) the corresponding overpressure in the gas phase is much higher in this case (1500 Pa for tangential, 105 000 Pa for radial). Even tough this higher overpressure leads to higher gradients of pressure within the material, drying is longer. Indeed, Fig. 18 shows that in the case of radial properties, drying is not yet fully accomplished after 30 min, the half of the particle remaining moist. In this case, drying requires 36 min to be complete.

Fig. 19 shows the internal profiles of temperature and wood concentration in both conditions under study (radial, tangential) during the pyrolysis period. As it was already observed in the preceding paragraphs, the thermal degradation seems soft compared to the drying steps. Overpressures (see also Figs. 17 and 12) are smaller and so are the gaseous concentrations. This means that the pyrolysis is much less dependent upon the transport of material than it is on the transport of heat. Hence, because thermal conductivity is higher in the case of "tangential properties" (0.35 W m^{-1} K^{-1}) than in the case of "radial properties" (0.55 W m^{-1} K^{-1}) the complete degradation of wood is faster in the first case (115 min) than in the second case (123 min).

4. Conclusion

A mathematical model devoted to the slow pyrolysis of a single and spherical particle of wood was presented in this study. This model mainly relies on the use of the method of volume averaging for the derivation of balance equations (mass, energy and momentum). This model incorporates the reaction pathway that was developed by Shafizadeh and Chin [8] for the description of the transformation of wood subject to heat. This model allows the computation of internal profiles of moisture content, chemical species concentration, temperature and pressure in the particle under study.

This work includes a validation section that shows the ability of the model to accurately predict the internal profiles of temperature in an experimental configuration depicted by Bilbao et al. [19]. Then the model is used in order to raise our knowledge on the mechanism responsible for the transformation of wood heated by hot nitrogen flowing around the particle under study. The use of the model clearly shows that the transformation is a succession of three important steps: drying, heating and pyrolysis. During drying, the temperature is stuck to the wet bulb temperature until the water content decreases. This prevents the occurrence of the pyrolysis step. An important conclusion is that in the studied configuration the drying step takes a third of the overall transformation process. The influence of transport parameters (i.e. thermal conductivity and permeability) is also investigated in this work. More precisely, this parametric study is devoted to the comparison between "radial" and "tangential" properties. The results obtained by the model in both situations clearly show the anisotropy of wood.

This work is the first step of our modelling effort devoted to the Chartherm© reactor. Indeed, this model for a single particle has to be incorporated in a global reactor model. This is exactly what is under investigation at the present time in our laboratory.

Acknowledgments

Because this research is supported by the Thermya company, the Association Nationale de la Recherche Technique and the Conseil Régional d'Aquitaine, the authors wish to thank these institutions for their contribution to this work.

Appendix A.

As it was discussed earlier, the mathematical model consists of a set of partial differential equations and algebraic equations. All differential equations were explained previously but only few algebraic equations were presented. To close the problem, we need additional algebraic equations.

A.1. Constants used in this model

A.1.1. Molecular weight

The molecular weight of the gaseous phase M_g is calculated as follows:

$$M_g = \langle \rho_g \rangle^g \left(\sum_{i=1}^{NGS} \frac{\langle \rho_i \rangle^g}{M_i} \right)^{-1} \quad (26)$$

where M_i is the molecular weight of the gaseous species i.

A.1.2. Intrinsic average density

Intrinsic average density of wood:

$$\langle \rho_W \rangle^W = 1500\,[\mathrm{kg/m^3}]$$

Intrinsic average density of char:

$$\langle \rho_c \rangle^c = 1500\,[\mathrm{kg/m^3}]\,(\text{measured by Thermya})$$

Intrinsic average density of free water:

$$\langle \rho_l \rangle^l = 1000\,[\mathrm{kg/m^3}]$$

Intrinsic average density of bound water:

$$\langle \rho_b \rangle^b = 1000\,[\mathrm{kg/m^3}]$$

A.1.3. Viscosity

Dynamic viscosity of free water:

$$\mu_l = 5 \times 10^{-4}\,[\mathrm{Pa\,s}]$$

A.2. Physical properties

A.2.1. Enthalpy

Eq. (21) defines the enthalpy using standard enthalpy of formation as a reference. Thus, this data is required for species present in the system as well as for "solid species". Also in order to compute the local value of the enthalpy using Eq. (21), the specific heat is required.

The standard enthalpy of formation for wood is computed according to the work of Boissonnet and Seiler [17]:

$$h^{\circ}_{Wf} = -7.6 \times 10^{6}\,[\mathrm{J/kg}]$$

Concerning char, we assume that it can be described as pure carbon, hence, its standard enthalpy of formation is equal to zero.

Grønli [7] reports the specific heat for wood and char as a function of temperature:

$$C_{P,W} = 1500 + T\,[\mathrm{J/(kg\,K)}]$$
$$C_{P,C} = 420 + 2.09 \times T + 6.85 \times 10^{-4} \times T^{2}\,[\mathrm{J/(kg\,K)}]$$

Specific heat and standard enthalpy of formation for free water and for each gaseous species present in the system are thermodynamic data available in the literature (JANAF tables for example).

Regarding the evaluation of the enthalpy to weight of bound water, it is necessary to give an expression for its heat of desorption ΔH_{sorp}. Ouelhazi et al. [20] report it as a function of the temperature and the bound moisture content:

$$\Delta H_{\mathrm{sorp}} = 400 \times (3174.9 - 2.46 \times T) \times (1 - M_{FSP}/M_b)^{2}\,[\mathrm{J/kg}]$$

Then, the bound water enthalpy is linked to the free water according to

$$\langle h_b \rangle^{b} = \langle h_l \rangle^{l} - \Delta H_{\mathrm{sorp}}$$

A.2.2. Viscosity of the gas phase

The gas phase is a multi-component phase whose composition is modified as drying and pyrolysis proceed.

The evaluation of the average viscosity of the gas μ_g is computed according to

$$\mu_g \langle \rho_g \rangle = \sum_{i}^{NSG} \mu_i \langle \rho_i \rangle \tag{27}$$

where μ_i stands for the viscosity of chemical species i, which is a function of temperature.

A.2.3. Thermal conductivity

According to the volume averaging theory, the local effective conductivity of the medium is computed according to

$$\lambda_{eff} = \varepsilon_W \lambda_W + \varepsilon_c \lambda_c + \varepsilon_l \lambda_l + \varepsilon_b \lambda_b + \varepsilon_g \lambda_g \tag{28}$$

As in the case of viscosity, the value of the thermal conductivity of the gas λ_g is computed according to

$$\lambda_g \langle \rho_g \rangle = \sum_{i}^{NSG} \lambda_i \langle \rho_i \rangle \tag{29}$$

where λ_i stands for the thermal conductivity of chemical species i, which is a function of temperature.

A.3. Intra-particular transports

A.3.1. Drying

As it was already quoted, the total moisture content M is defined as the ratio of the total concentration of water (free, bound and vapour) to the wood concentration:

$$M = \frac{\langle \rho_l \rangle + \langle \rho_b \rangle + \langle \rho_{\mathrm{H_2O(g)}} \rangle}{\langle \rho_w \rangle} \tag{30}$$

$\langle \rho_{\mathrm{H_2O(g)}} \rangle$ is computed assuming that there is an equilibrium between the liquid phase and the gaseous one.

$$\langle \rho_{\mathrm{H_2O(g)}} \rangle = \varepsilon_g \frac{\langle P_{\mathrm{H_2O(g)}} \rangle^{g} M_{\mathrm{H_2O}}}{R_g \langle T \rangle} \tag{31}$$

where $\langle P_{\mathrm{H_2O(g)}} \rangle^{g}$ is a function of $P^{\mathrm{sat}}_{\mathrm{H_2O(g)}}$ the pressure of saturation of pure water and a_w the activity of water (Eq. (1)).

A.3.2. Convection

Darcy's law is assumed to compute the velocity of the gas phase $\mathbf{v_g}$ and the velocity of the liquid water $\mathbf{v_l}$:

$$\langle \mathbf{v_g} \rangle = -\frac{K_g K_r^{g}}{\mu_g} \nabla \langle P_g \rangle^{g} \tag{32}$$

$$\langle \mathbf{v_l} \rangle = -\frac{K_l K_r^{l}}{\mu_l} \nabla \langle P_l \rangle^{l} \tag{33}$$

The gas pressure $\langle P_g \rangle^{g}$ is computed according to the ideal gas law and the pressure in the liquid phase $\langle P_l \rangle^{l}$ is linked to the capillary pressure by Eq. (16).

Relative permeabilities characterize the interactions between the flows of different phases.

Based on experimental data, simplified models of relative permeability as a function of moisture content can be constructed. An usual approximation is the so-called Corey type, which is polynomial in the water saturation. In this work, the relations developed by Perre et al. [21] were used:

$$\begin{aligned} &\text{Radial direction}: \; K_r^{l} = \left(\frac{M_l}{M_{lsat}}\right)^{3} \quad K_r^{g} = 1 + \left(2\frac{M_l}{M_{lsat}} - 3\right)\left(\frac{M_l}{M_{lsat}}\right)^{2} \\ &\text{Tangential direction}: \; K_r^{l} = \left(\frac{M_l}{M_{lsat}}\right)^{8} \quad K_r^{g} = 1 + \left(4\frac{M_l}{M_{lsat}} - 5\right)\left(\frac{M_l}{M_{lsat}}\right)^{4} \end{aligned} \tag{34}$$

where M_l stands for the free liquid content and M_{lsat} represents the maximum amount of water that wood might hold:

$$\begin{aligned} \varepsilon_g &= 1 - \left(\frac{\langle \rho_W \rangle}{\langle \rho_W \rangle^{W}} + \frac{\langle \rho_l \rangle}{\langle \rho_l \rangle^{l}} + \frac{\langle \rho_b \rangle}{\langle \rho_b \rangle^{b}}\right) = 0 \Rightarrow M_{lsat} = \frac{\langle \rho_l \rangle + \langle \rho_b \rangle}{\langle \rho_W \rangle} \\ &= \langle \rho_l \rangle^{l} \left(\frac{1}{\langle \rho_W \rangle} - \frac{1}{\langle \rho_W \rangle^{W}}\right) \end{aligned} \tag{35}$$

In the different calculations, we have fixed the other permeabilities to

$$K_l = 5 \times 10^{-16}\,[\mathrm{m^2}] \text{ (radial direction)};$$

$$K_l = 5 \times 10^{-13}\,[\mathrm{m^2}] \text{ (tangential direction)};$$

$$K_g = \eta \times 5 \times 10^{-16} + (1 - \eta) \times 10^{-10}\,[\mathrm{m^2}] \text{ (radial direction)};$$

$$K_g = \eta \times 5 \times 10^{-13} + (1 - \eta) \times 10^{-10}\,[\mathrm{m^2}] \text{ (tangential direction)}$$

where η is the interpolation factor, defined by the ratio between the wood concentration and the initial wood concentration.

For capillary pressure, Perre et al. [21] estimated that it was linked both to temperature and local moisture content:

$$Pc = 1.64 \times 10^{5} \times (128 - 0.185 \times T) \times (M_l + 1.2 \times 10^{-4})^{-0.63}\,[\mathrm{Pa}]$$

A.3.3. Diffusion

Bound water transport is often described as a Fick's diffusional transport:

$$\langle \rho_b \mathbf{v_b} \rangle = -\langle \rho_W \rangle D_b \nabla \left(\frac{\langle \rho_b \rangle}{\langle \rho_W \rangle}\right) \tag{36}$$

Perre et al. [21] express bound water transport by considering the diffusion coefficient of bound water D_b as a function of temperature and bound water moisture content:

$$D_b = \exp(-9.9 + 9.8 \times M_b - 4300/T)\,[\mathrm{m^2/s}] \text{ (radial direction)} \tag{37}$$

$$D_b = 2.5 \times \exp(-9.9 + 9.8 \times M_b - 4300/T)\,[\mathrm{m^2/s}] \quad (\text{tangential direction}) \tag{38}$$

Diffusional transport of gaseous species within the particle is more complex to express. In order to take into account potential interactions with the wood fibres, diffusion coefficients are corrected with the introduction of the tortuosity of the material. Usually introduced for the design of catalytic reactors, the following expression allows the estimation of the binary effective diffusion coefficient D_{eff}^{ij} as a function of the material tortuosity τ and the binary diffusion coefficient D^{ij}:

$$D_{eff}^{ij} = \frac{D^{ij}}{\tau}\,[\mathrm{m^2/s}] \tag{39}$$

Jacobson [22] fixes the tortuosity of pine wood to 1.6.

The estimation of the mutual diffusion coefficients D^{ij} is also quite complex. To simplify the problem, we have assumed that the gas is mainly composed of nitrogen and we have considered a binary diffusion transport:

$$D_{eff}^{i} = D_{eff}^{iN_2} = \frac{D^{iN_2}}{\tau}\,[\mathrm{m^2/s}] \quad (\text{case } j = N_2) \tag{40}$$

In Treybal [23], Wilke–Lee modification of Hirschfelder–Bird–Spottz method is presented. It gives the binary diffusion coefficient D_{ij} as a function of the temperature and the pressure.

A.4. External transport

A.4.1. Heat transfer coefficient

Concerning external heat transfer, the correlation given by Necati Ozisik [24] was used:

$$Nu = 2 + (0.4Re^{0.5} + 0.06Re^{2/3})Pr^{0.4}\left(\frac{\mu_{\mathrm{inf}}}{\mu_{\mathrm{surf}}}\right)^{0.25} \tag{41}$$

A.4.2. Mass transfer coefficient

Each mass transfer coefficient will be deducted from the Sherwood number:

$$Sh = 2 + (0.4Re^{0.5} + 0.06Re^{2/3})Sc^{0.4}\left(\frac{\mu_{\mathrm{inf}}}{\mu_{\mathrm{surf}}}\right)^{0.25} \tag{42}$$

where Sh represents the Sherwood number and Sc the Schmidt number.

References

[1] P. Duverneuil, B. Fenouillet, C. Chaffot, Récupération des métaux lourds dans les déchets et boues issus des traitements des effluents, Lavoisier Tec & Doc, 1997.
[2] L.M. Helsen, The Chartherm process, what's in the name? Waste Management 29 (2008).
[3] K.M. Bryden, K.W. Ragland, C.J. Rutland, Modeling thermally thick pyrolysis of wood, Biomass and Bioenergy 22 (2002) 41–53.
[4] C. Di Blasi, Analysis of convection and secondary reaction effects within porous solid fuels undergoing pyrolysis, Combustion Science and Technology 90 (1993) 315–340.
[5] S. Whitaker, Simultaneous heat, mass, and momentum transfer in porous media: a theory of drying, Advances in Heat Transfer 13 (1977) 119–203.
[6] R. Reid, J. Prausnitz, J. Poling, The Properties of Gases and Liquids, fourth edition, McGraw-Hill, 1987.
[7] M. Grønli, A theoretical and experimental study of the thermal degradation of biomass, Ph.D. Thesis, The Norwegian University of Science and Technology, 1996.
[8] F. Shafizadeh, P.S. Chin, Thermal deterioration of wood, wood technology: chemical aspects, ACS Symposium Series 43 (1977) 57–81.
[9] F. Thurner, U. Mann, Kinetic investigation of wood pyrolysis, Industrial Engineering Chemistry Process Design and Development 20 (1981) 482–488.
[10] A.C. Liden, F. Berruti, D.S. Scott, A kinetic model for the production of liquids from the flash pyrolysis of biomass, Chemical Engineering Communications 65 (1988) 207–221.
[11] C. Di Blasi, Modeling and simulation of combustion processes of charring and non-charring solid fuels, Progress in Energy and Combustion Science 19 (1993) 71–104.
[12] W-C.R. Chan, M. Kelbon, B.B. Krieger, Modelling and experimental verification of physical and chemical processes during pyrolysis of a large biomass particle, Fuel 64 (1985) 1505–1513.
[13] S.D. Glaister, The prediction of chemical kinetic, heat, and mass transfer processes during the one and two dimensional pyrolysis of a large wood pellet, Ph.D. Thesis, University of Washington, 1987.
[14] M.R. Hajaligol, J.B. Howard, J.P. Longwell, W.A. Peters, Product compositions and kinetics for rapid pyrolysis of cellulose, Industrial & Engineering Chemistry Process Design and Development 21 (1982) 457–465.
[15] S. Baumlin, Craquage thermique des vapeurs de la pyrolyse-gazéification de la biomasse en réacteur parfaitement auto-agité par jets gazeux, Ph.D. Thesis, Institut national Polytechnique de Lorraine, 2006.
[16] V. Repellin, Optimisation des paramètres durée et température d'un traitement thermique du bois. Modifications des propriétés d'usage du bois en relation avec les modifications physico-chimiques et ultrastructurales occassionnées par le traitement, Ph.D. Thesis, Ecole Nationale Suupérieure des Mines de Saint-Etienne, 2006.
[17] G. Boissonnet, J.-M. Seiler, Approche thermodynamique des transformations de biomasse, Rapport CEA, 2003.
[18] A. Erriguible, Modélisation des transferts à l'interface d'un milieu multiphasique et son environnement, Ph.D. Thesis, Université de Pau et des Pays de l'Adour, 2004.
[19] R. Bilbao, A. Millera, M.B. Murillo, Temperatures profiles and weight loss in the thermal decomposition of large spherical wood particles, Industrial & Engineering Chemistry 32 (1993) 1811–1817.
[20] N. Ouelhazi, G. Arnaud, J.P. Fohr, A two-dimensional study of wood plank drying: effect of gaseous pressure below boiling point, Transport Porous Media 7 (1992) 39–61.
[21] P. Perre, I. Turner, The use of macroscopic equations to simulate heat and mass transfer in porous media: some possibilities illustrated by a wide range of configurations that emphasise the role of internal pressure simultaneous heat, mass, and momentum transfer in porous media: a theory of drying, in: Ian Turner, Arun S. Mujumdar (Eds.), Mathematical Modelling and Numerical Techniques in Drying Technology, Marcel Dekker, Inc., New York, 1997.
[22] A. Jacobson, Diffusion of chemicals in green wood, Ph.D. Thesis, Georgia Institute of Technology, 2006.
[23] R. Treybal, Mass Transfer Operations, third edition, McGraw-Hill Chemical Engineering Series, 1980.
[24] M. Necati Ozisik, Heat Transfer: A Basic Approach, McGraw-Hill, 1985.